FIRST DATA RELEASE OF THE ALL-SKY NOAO SOURCE CATALOG

David L. Nidever[1,2], Arjun Dey[2], Knut Olsen[2], Stephen Ridgway[2], Michael Fitzpatrick[2] and Adam Scott[2]
Draft version January 9, 2018

ABSTRACT

Most of the sky has been imaged with NOAO's telescopes from both hemispheres. While the large majority of these data were obtained for PI-led projects only a small fraction have been released to the community via well-calibrated and easily accessible catalogs. We are remedying this by creating a catalog of sources from most of the public data taken on CTIO-4m+DECam as well as KPNO-4m+Mosaic3. This catalog, called the NOAO Source Catalog (NSC), already contains over 2.9 billion unique objects, 34 billion source measurements, covers ~30,000 square degrees of the sky, has depths of ~23rd magnitude in most broadband filters with ~1–2% photometry, and astrometric accuracy of ~2 mas. The NSC will be useful for exploring stellar streams, dwarf satellite galaxies, as well as variable stars and other transients. We release the catalog via the new NOAO Data Lab service in January 2018.

Subject headings: catalogs

1. INTRODUCTION

It has been clear for more than a decade that astronomy is in a period of rapid expansion of collected data volume (Brunner et al. 2002). This development is evident in the evolution from the NOAO Deep Wide-Field Survey (NDWFS; Jannuzi & Dey 1999), through the Sloan Digital Sky Survey (SDSS; York et al. 2000), to Pan-STARRS1 (PS1; Magnier et al. 2016).

The trend continues into the future with the Dark Energy Survey (DES; Dark Energy Survey Collaboration et al. 2016), the Zwicky Transient Factory (ZTF; Bellm et al. 2015), and the Large Synoptic Survey Telescope (LSST; Ivezic et al. 2008). The growth of Big Data in astronomy can be correctly described as exponential (Zhang & Zhao 2015) — a fact that has attracted the attention even of the lay press (Atlantic Monthly 2012). These future mega-surveys will define a new astronomical data landscape, with an unprecedented combination of coverage and uniformity.

As the community works to evolve astronomy into an increasingly archival and data-intensive science, it faces a conundrum of how to prepare for a research environment that does not yet exist. Conferences, schools and seminars proliferate. Working groups prepare with multi-year lead times for both narrow and broad science opportunities foreseen for the next decade (e.g., LSST Science Collaborations[3]).

Meanwhile, as the community prepares for that era, currently existing and growing data resources offer great potential for immediate analysis, and for exploration and preparatory programs. A few major archives, such as SDSS[4], play an essential role, offering challenging opportunities that can be studied with the most modern data mining and computer learning methodology, developing expertise, experience, and crucially, produce science results now — an essential ingredient for a healthy science demographic.

It is perhaps not so well known that the cumulative product of several major observing facilities on Kitt Peak and Cerro Tololo have, over the years, delivered a high quality, broad coverage imaging data set with standard filters. Though intended for a variety of science programs, these data have a considerable degree of homogeneity. However, obtained under different protocols and by multiple PI's, the data have not been conveniently accessed and simply merged. Recognizing the potential inherent in these massive data, we have undertaken to convert them into a unified, public database. By reprocessing the raw data, with consistent quality control, selection, calibration and documentation, we have merged these data as the NOAO Source Catalog (NSC). Reductions have utilized proven tools and methodologies, adapted to the extant data materials. Careful attention has been paid to crowding, PSF and image shape, photometric calibration and astrometric zero points.

The NSC is now "open for business", with over 255,000 exposures and 2.9 billion unique objects (Figure 1). The NSC may be accessed through NOAO's Data Lab, with tools for discovery, image cutout, and supported Jupyter notebook analysis, and also by direct query or TAP service.

With a recognized trajectory for extensions and improvements, the NSC will be updated continuously as new material is added, as more advanced processing can be implemented, and as the database is further adapted to client needs.

2. DATASET

The large majority of the NSC data are from the Dark Energy Camera (DECam) on the CTIO-4m with over 195,000 exposures used in NSC DR1. The NOAO Science Archive also contains a large number of public data for the DESI Legacy Survey[5] including *z*-band images from KPNO-4m+Mosaic-3 (Mosaic-3 Legacy Survey; MzLS; Dey et al. 2016) and *g* and *r*-band image from Bok-

---

[1] Department of Physics, Montana State University, P.O. Box 173840, Bozeman, MT 59717-3840 (dnidever@montana.edu)
[2] National Optical Astronomy Observatory, 950 North Cherry Ave, Tucson, AZ 85719
[3] https://www.lsstcorporation.org/node/37
[4] http://www.sdss.org
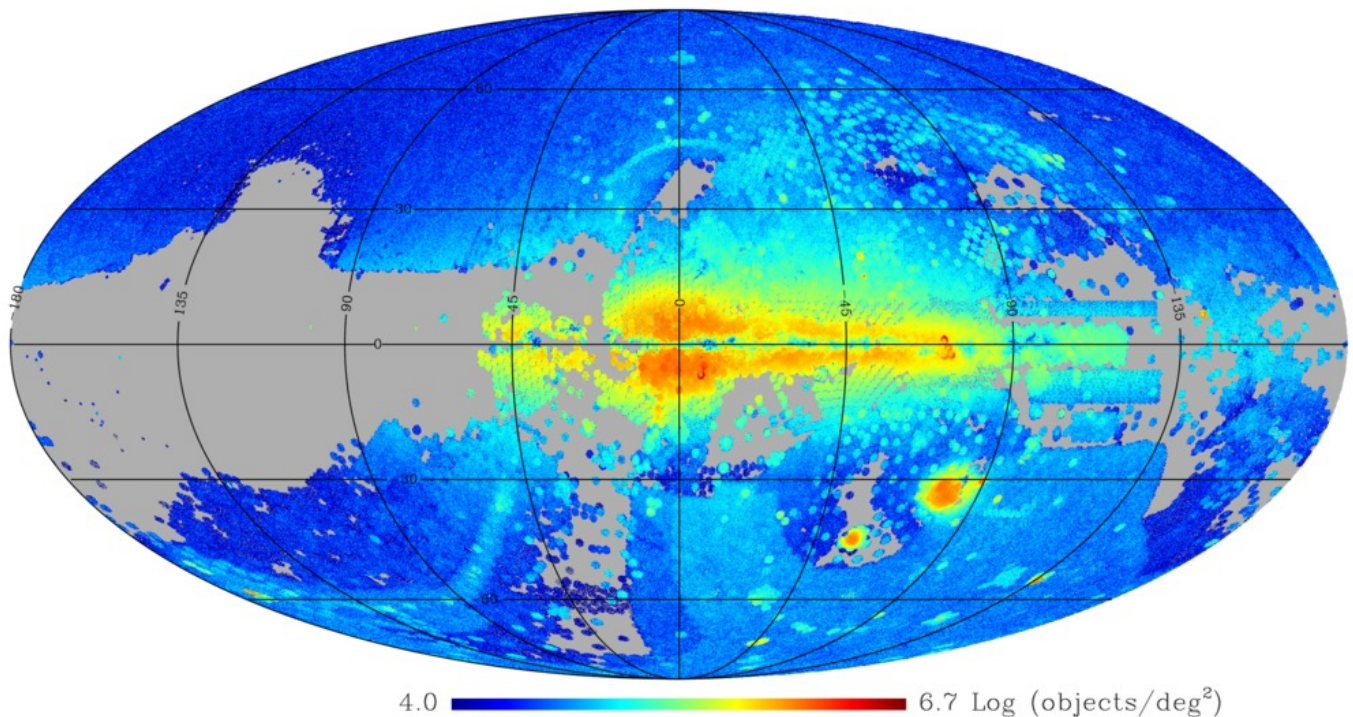
[5] http://legacysurvey.org

Fig. 1.— Density of the 2.9 billion NSC objects on the sky in Galactic coordinates.

2.3m+90Prime (Beijing-Arizona Sky Survey; BASS; Zou et al. 2017). The MZLS and BASS data cover a good fraction of the northern sky and were also included in NSC DR1.

Older Mosaic-1, 1.1 and 2 images have not been added to the NSC yet mainly because of the difficulty of photometrically calibrating so many different filters. We are investigating means of including these in future versions of the NSC.

3. REDUCTION AND PHOTOMETRY

The NSC data processing makes use of three separate software packages: (1) the NOAO Community Pipeline (CP; Valdes et al. 2014)[6] for instrument signature removal, (2) Source Extractor[7] (Bertin & Arnouts 1996) for performing source extraction from the images, and (3) custom software[8] (in python and IDL) to run SExtractor on the images and to perform calibration and combination.

All of the images were reduced by the NOAO Community Pipeline. The instrumentally calibrated ("Inst-Cal") images with the instrumental signature removed were used for further analysis to create the NSC catalogs.

3.1. *Measurement*

Several software packages were considered to perform the photometric source extraction. Source Extractor (SExtractor) was chosen because it is well tested, produces source morphology parameters (which is useful for galaxy science), is fast, and can give useful results in crowded regions if tuned properly.

SExtractor was run on each individual chip CP "flux" image to extract aperture photometry and morphological parameters. The CP "weight" images were used for the SExtractor WEIGHT_IMAGE and the weights were set to zero for pixels masked as bad (non-zero) in the CP "quality mask" image. A WEIGHT_THRESH=1×10^{-8} was used to indicate to SExtractor to ignore the bad pixels. The CP quality mask image was also used for the FLAG_IMAGE to give mask information for individual sources. The CP mask flags were converted to bitmasks (see Table 1) and homogenized across the various CP versions and are similar to the Pre-V3.5.0 CP flags. The V3.5.0 CP values are integers and are not properly interpreted by SExtractor especially when combining values across pixels in a source footprint. The SExtractor configuration parameters[9] were modified slightly for each image (seeing, gain, saturation level and circular aperture sizes).

One of the goals of the NSC (as for most surveys) is to achieve uniformity across the survey in the detection

<div style="text-align:center">

TABLE 1
CP BITMASK FLAGS

</div>

Bit	Value	Condition
1	1	Bad pixel
2	2	not used
3	4	Saturated
4	8	Bleed mask
5	16	Cosmic ray
6	32	Low weight
7	64	Diff detect

limit (e.g., 5σ) for all filters and seeing conditions but to also perform well in crowded and uncrowded regions. Accomplishing both of these goals simultaneously is challenging. The best detection is achieved when the image is smoothed with a kernel the size of the PSF (Bijaoui & Dantel 1970). However, for poor seeing exposures in crowded regions this smoothing can cause a very large fraction of the pixels in the image to be blended together and produces difficulties for the deblender. Therefore, it was decided to use a consistent smoothing kernel (FWHM=4 pixels) and detection threshold ($1.1\times$ the background noise) for all exposures that would give a $\sim5\sigma$ detection limit for the median seeing ($\sim1.26''$) images (for DECam and Mosaic3) and would also not overwhelm the deblender in the most crowded regions. Variations on this scheme will be evaluated for future versions of the NSC.

We discovered that when smoothing ("filtering") an image in SExtractor that pixels marked as "bad" (using the WEIGHT_LIMIT flag) grow and affect nearby pixels. This essentially masks out larger regions around bad pixels and bad columns and adversely affects certain computed source quantities. To be able to remove the affected sources using the output flags, bad pixels were artificially grown in the same manner in the mask ("flag") image.

We use the SExtractor automatic aperture magnitudes (MAG_AUTO) which estimates the magnitude in an elliptical aperture defined by a source's morphology.

3.2. Calibration

3.2.1. Astrometry

Gaia DR1 data were used to astrometrically calibrate each chip independently. Crossmatches were found between the NSC sources and Gaia DR1 sources using a $0.5''$ matching radius and then the coordinates of both groups were transformed into a tangent plane projection using the center of the chip (RA and DEC in the chip table) giving ζ (α direction) and η (δ direction). Linear additive correction coefficients in both ζ and η were then determined for both α and δ:

α corr = RA_COEF1 + RA_COEF2$\times\zeta$ + RA_COEF3$\times\zeta\eta$ + RA_COEF4$\times\eta$

δ corr = DEC_COEF1 + DEC_COEF2$\times\zeta$ + DEC_COEF3$\times\zeta\eta$ + DEC_COEF4$\times\eta$

These coefficients are also given in the chip table. A robust standard deviation (using the median absolute deviation) and a robust standard deviation of the mean (e.g. robust standard deviation divided by $\sqrt{(N)}$) are calculated for the residuals in α (RARMS, RASTDERR) and δ (DECRMS, DECSTDERR). The median RMS value in α/δ is 22 mas and the median standard deviation of the mean is 1.9 mas. There are roughly 200 Gaia DR1 matches per chip that are used for astrometric calibration.

3.2.2. Photometry

For large datasets like the NSC, it is challenging to use the classical calibration method of standard star fields to derive photometric transformation equations because this is often a manual and time-consuming process. Instead, it is more common to derive zero points for each exposure (or CCD image) by using existing catalogs in the same area of the sky and in the same filters. Since there is currently no existing large-scale, public survey in optical broadband filters in the southern hemisphere, this option was not a possibility for a large fraction of our data which is in the southern hemisphere. For the NSC, we decided instead to construct model magnitudes for our filters (u, g, r, i, z, Y, VR) from public all-sky catalogs (valid for certain color ranges) and an extinction term. This technique is similar to that used for the "real-time calibration" performed by Pan-STARRS1 (PS1; Magnier et al. 2016). A number of public catalogs were examined but the final set contained 2MASS (Skrutskie et al. 2006), Gaia DR1 (Gaia Collaboration et al. 2016), APASS (Henden et al. 2015), and GALEX (Bianchi et al. 2011) with the Schlegel, Finkbeiner & Davis (1998) reddening map for the extinction term. The model magnitude coefficients were determined in two steps:

1. The best model magnitudes were determined by comparing a superposition of the public all-sky catalogs to the photometric reference catalog (that set the zero point of the photometric system; PS1 for $grizY$, SMASH for u-band and Gaia G for VR). Data from the Stripe82 region ($-60°<\alpha<+60°$, $-1.1°<\delta<1.1°$) were used to determine the coefficients (except for u-band which used 41 SMASH fields).

2. The NSC exposures in the Stripe82 region were calibrated (and combined) using the coefficients determined in step 1. The calibrated NSC magnitudes were then compared to the model magnitudes and inspected for residual color terms that could arise from the differences in the PS1 and DECam filters. The model magnitude coefficients were adjusted to remove the residual patterns but the mean values were kept the same to remain on the photometric scale of the reference catalogs.

The residuals (from step 2) versus color are shown in Figure 2 and the final model magnitude coefficients are presented in Table 2. Figure 2 also shows the model magnitude color ranges used to determine the zero points which were determined by selecting the color region in the residuals where the systematics were small. The PS1 photometry was used to determine the zero points for $grizY$ exposures with $\delta>-29°$ which included all of the data from Mosaic-3 and 90Prime.

Exposure-level zero points were used because the density of some of the catalogs needed to construct the model magnitudes was too low (especially APASS) to determine
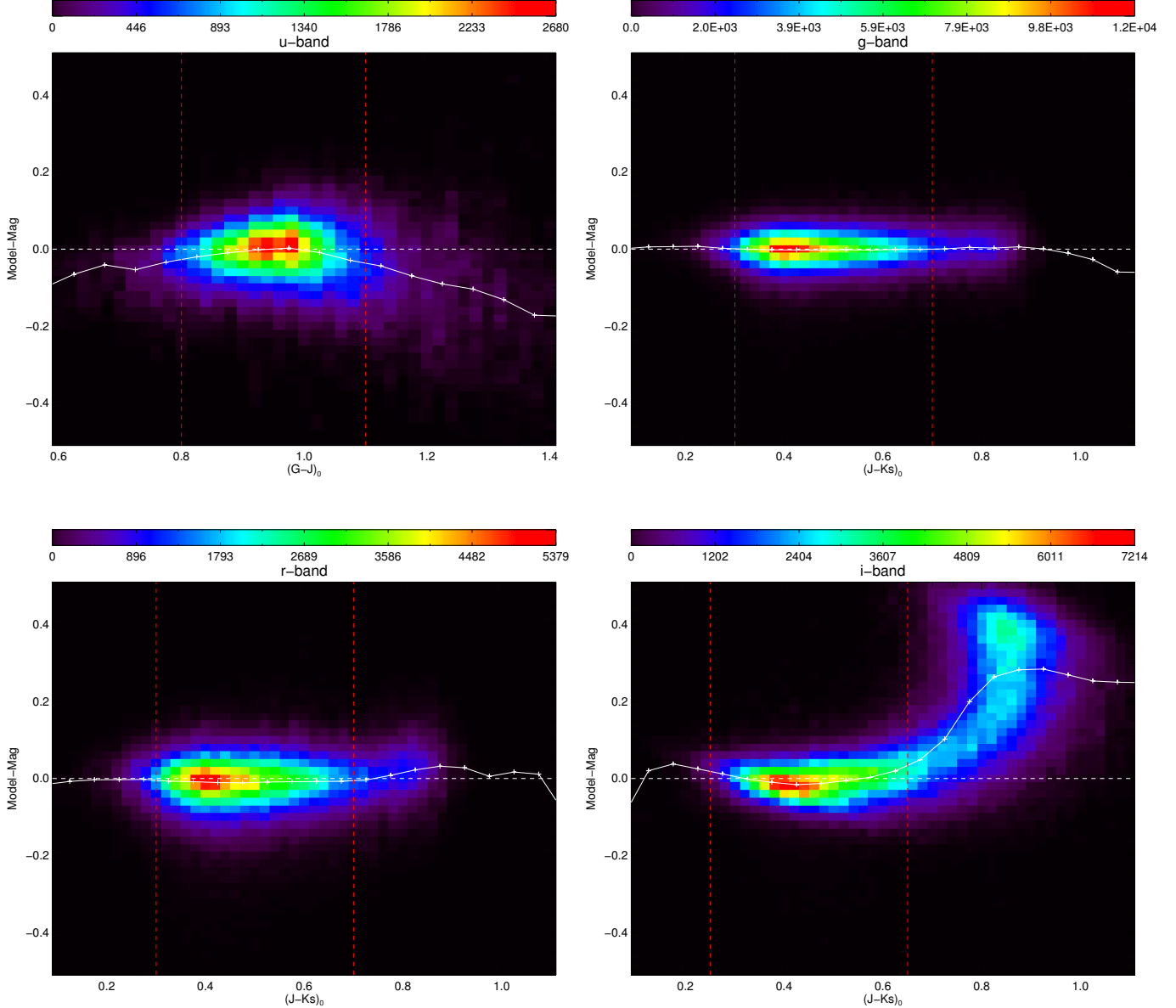
FIG. 2.— Model magnitude figures with panel per band. Density image of residual magnitude vs. color. The median values in color bins are shown as white crosses and connected with solid white lines. The color ranges used to determine the zero-point per exposure are indicated by the two vertical white dotted lines.

accurate chip-level zero points. However, chip-level zero points were computed when possible (≥ 5 reference objects per chip) in order to estimate spatial variations in zero points across an exposure that could indicate non-photometric conditions. Even with exposure-level zero points, some exposures failed due to a lack of good photometric reference stars. In these instances, well-calibrated, overlapping NSC exposures in the same filter were used to obtain the zero point (ZPTYPE=2 in the exposure table). Table 3 gives statistics on the zero point scatter and uncertainties per filter showing that the random uncertainties on the zero points are quite small.

3.3. Combination

The data are crossmatched and combined in the final stage of the NSC processing. A healpix scheme is used (nside=128 with ~0.21 square degrees per pixel and ring ordering) to fully tile the sky and allow for more efficient parallelization of the combination step. Before the processing is initiated, exposure-level quality cuts are applied to all exposures that successfully completed the calibration step. These cuts are:

- Public data.

- Astrometrically calibrated by the CP.

- All chips astrometrically calibrated in NSC calibration step.
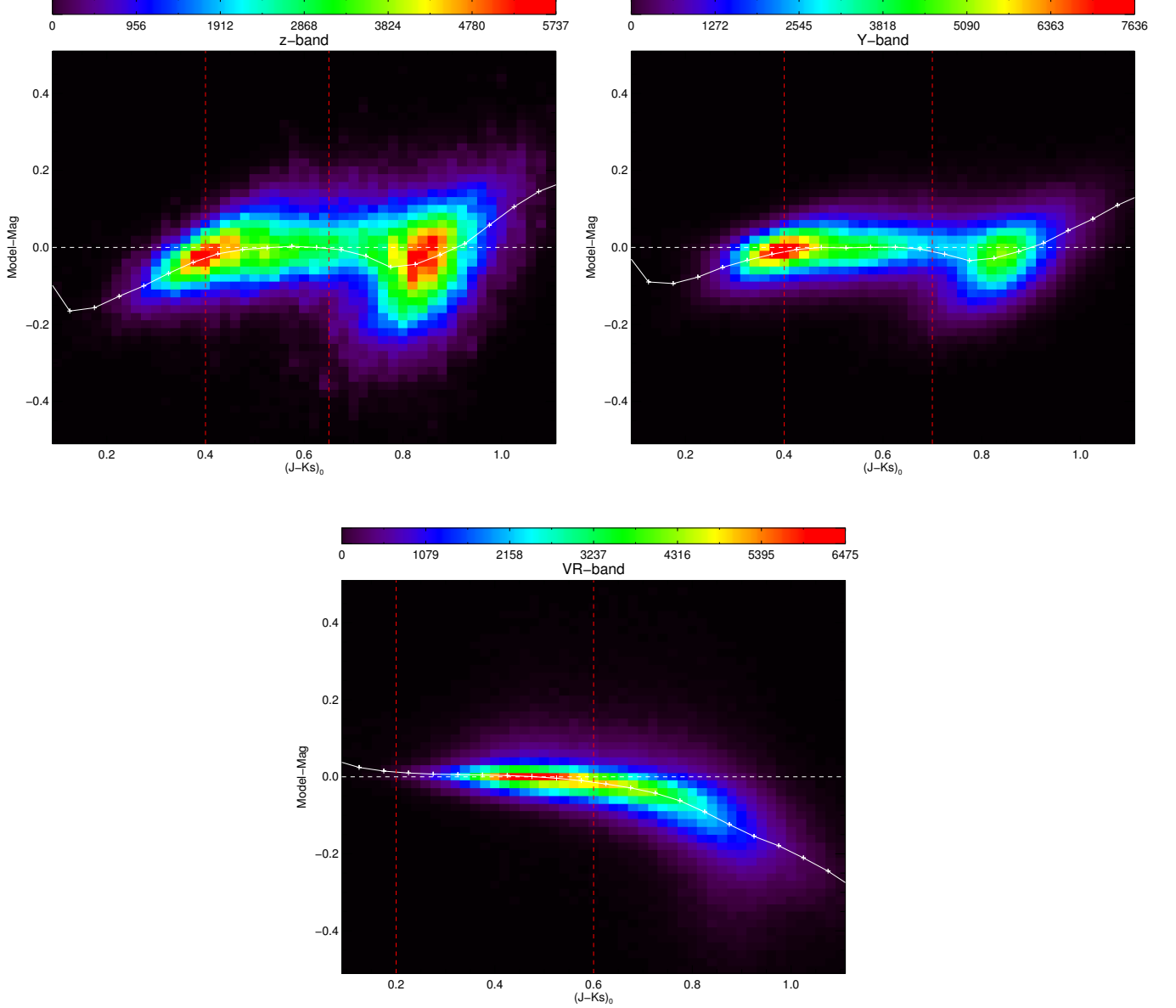
Fig. 2.— (cont.)

- Median α/δ RMS across all chips $\leq 0.15''$.

- Seeing FWHM $\leq 2''$.

- Zero point (corrected for airmass extinction) within 0.5 mag of the temporally-smoothed median zero point for that band.

- Zero point uncertainty ≤ 0.05 mag.

- Number of photometric reference stars ≥ 5.

- Spatial variation (RMS across chips) of zero point ≤ 0.1 mag (only for DECam with number of chips with well-measured chip-level zero points >5).

- Not in survey bad exposure list (currently only Legacy Survey and SMASH).

Then the final list of exposures and the healpix pixels that they overlap is created.

For any given healpix pixel all exposures overlapping it and its neighboring pixels are successively loaded. Only sources of an exposure that fall within $10''$ of the healpix pixel boundary are kept. Source-level quality cuts are also applied:

- No CP mask flags set.

- No SExtractor object or aperture truncation flags.

- Remove sources in bad amplifier of DECam CCD-NUM 31 (if MJD<56,600 or big background jump between amplifiers).

- S/N≥ 5.

Sources are successively crossmatched (with a $0.5''$ matching radius) to existing "objects" or are added

TABLE 2
NSC Model Magnitude Equations

Model Magnitude	Color Range
$u = 0.247 \times NUV_{\mathrm{GALEX}} + 0.75 \times G_{\mathrm{Gaia}} + 0.54 \times (G - J)_0 + 0.68 \times E(B - V) + 0.005$	$0.8 < (G - J)_0 < 1.1$
$g = g_{\mathrm{APASS}} - 0.0421 \times (J - K_{\mathrm{s}})_0 - 0.05 \times E(B - V) - 0.0620$	$0.3 < (J - K_{\mathrm{s}})_0 < 0.7$
$r = r_{\mathrm{APASS}} - 0.086 \times (J - K_{\mathrm{s}})_0 + 0.0 \times E(B - V) + 0.054$	$0.3 < (J - K_{\mathrm{s}})_0 < 0.7$
$i = G_{\mathrm{Gaia}} - 0.45 \times (J - K_{\mathrm{s}})_0 - 0.27 \times E(B - V) + 0.096$	$0.25 < (J - K_{\mathrm{s}})_0 < 0.65$
$z = J + 0.76 \times (J - K_{\mathrm{s}})_0 + 0.40 \times E(B - V) + 0.60$	$0.4 < (J - K_{\mathrm{s}})_0 < 0.65$
$Y = J + 0.54 \times (J - K_{\mathrm{s}})_0 + 0.20 \times E(B - V) + 0.66$	$0.4 < (J - K_{\mathrm{s}})_0 < 0.7$
$VR = G_{\mathrm{Gaia}}$	$0.2 < (J - K_{\mathrm{s}})_0 < 0.6$

$(G - J)_0 = G_{\mathrm{Gaia}} - J - 1.12 \times E(B - V)$
$(J - K_{\mathrm{s}})_0 = J - K_{\mathrm{s}} - 0.17 \times E(B - V)$

TABLE 3
Zero Point Statistics

Filter	δ Range	Median ZP RMS	Median ZP Error	N_{ref}
u	all	0.064	0.0099	129
g	> -29	0.041	0.0007	3994
g	< -29	0.032	0.0043	439
r	> -29	0.057	0.0010	5829
r	< -29	0.049	0.0080	254
i	> -29	0.082	0.0013	5646
i	< -29	0.056	0.0017	1370
z	> -29	0.076	0.0027	1749
z	< -29	0.078	0.0027	898
Y	> -29	0.037	0.0007	4144
Y	< -29	0.055	0.0017	968
VR	all	0.017	0.0007	804

as new objects if no match is found. Cumulative values of quantities are accumulated throughout this process and converted to average values at the very end. Most quantities such as morphology parameters are straight averages while coordinates and magnitudes per band are S/N-weighted averages. Average morphology values are computed per band and across all bands. Proper motions are computed as S/N-weighted least-squared fits but it should be noted that these are only relative to the foreground stars that are used to astrometrically calibrate each exposure to Gaia DR1. Also, the proper motions are effectively limited to $\lesssim 200$ mas yr^{-1} (although this depends on the cadence) because the multiple measurements from higher proper motion stars are "missed" owing to the $0.5''$ matching radius. Photometric RMS values per band across the multiple measurements are also computed and can be used to ascertain the photometric variability of an object. Only objects with final average coordinates within the boundary of the healpix pixel are kept.

4. DESCRIPTION AND ACHIEVED PERFORMANCE OF FINAL CATALOG

Figure 1 shows the density of the 2.9 billion objects in the NSC DR1 catalog covering $\sim 30,000$ square degrees. There are 34 billion measurements from 255 thousand exposures. Figure 3 shows maps of the 95th percentile depths in each of the seven bands. The median depth in each band is 23.1, 23.3, 23.2, 22.9, 22.2, 21.0, 23.1 mag in u, g, r, i, z, Y, and VR, respectively. The photometric

RMS of bright stars in regions with many exposures is $\lesssim 1\%$ in all bands except for u-band where it is $\sim 2\%$ indicating the precision of the NSC photometry. Finally, Figure 4 shows a map of the number of exposures and Figure 5 shows a cumulative histogram of the number of objects and area with a certain number of exposures or greater. A significant area on the sky and number of objects have multiple measurements that are useful for time-series science.

The NSC data are released through the NOAO Data Lab[10]. Access and exploration tools include the Data Lab Data Discovery tool, database access to the catalog (via direct query or TAP service), an image cutout service, and a Jupyter notebook server with example notebooks for exploratory analysis.

Figure 6 shows a comparison of the NSC photometry with the SMASH (Nidever et al. 2017) photometry for a healpix pixel in a crowded field only 2.4° from the LMC center. The SMASH CMD is deeper because it uses forced PSF photometry with detection on a multi-band stacked image and the stellar population features are sharper due to the lower photometric uncertainties from the PSF photometry. However, most of the important features are still visible in the CMD using the NSC aperture photometry in this crowded field. A direct g-band one-to-one comparison of crossmatched SMASH and NSC objects in the healpix pixel 144896 is shown in Figure 7. The photometry compares well for point sources with low FWHM (light blue) while they deviate for extended sources as expected because SMASH only has PSF photometry. Even for point sources there is a slight magnitude offset because SMASH and NSC are on slightly different photometric systems.

Figure 8 shows a comparison of the NSC proper motions to those in UCAC5 (Zacharias et al. 2017). The two datasets compare well with a small number of outliers at low UCAC5 proper motion values but higher NSC values.

There are six NSC DR1 tables in the database:

- **Coverage**. Coverage information for each nside=4096 healpix pixel with a resolution of $\sim 1'$. This gives the coverage fraction and depth for each band. 201,326,592 rows.
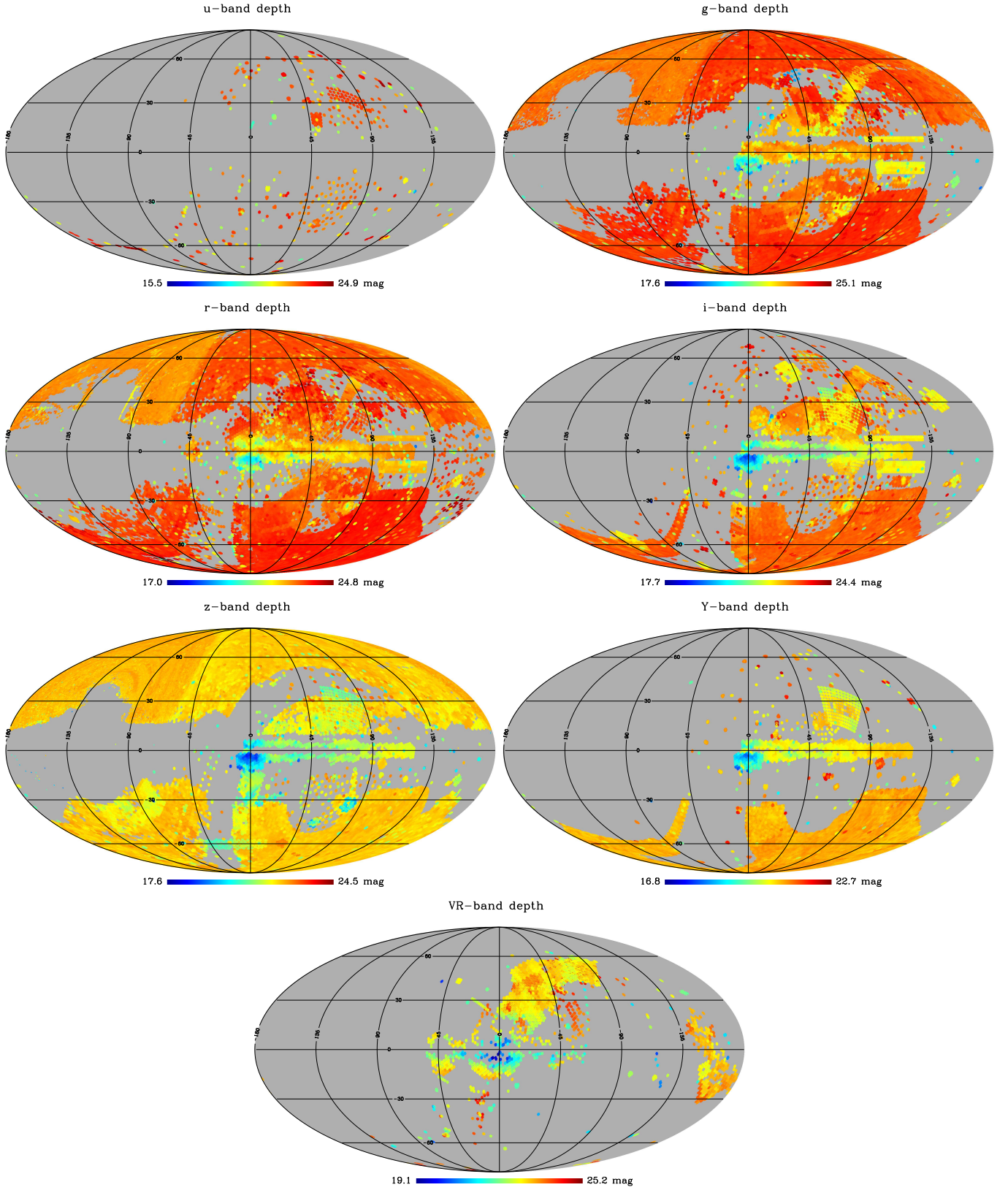
---

[10] http://datalab.noao.edu

FIG. 3.— Depth maps (95th percentile) for all seven u, g, r, i, z, Y and VR bands in Aitoff projection.
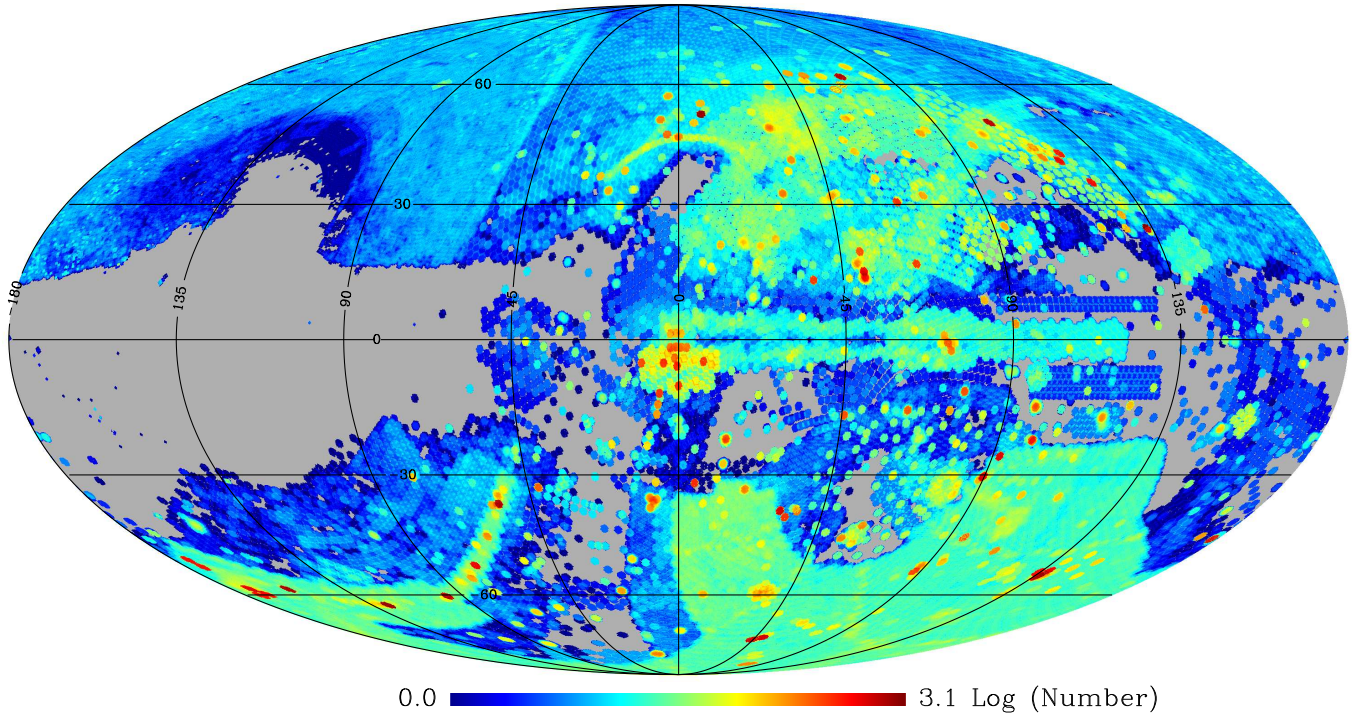
Number of Exposures

Fig. 4.— Number of NSC exposures on a logarithmic scale in Galactic coordinates.

- **Chip**. Information for each unique chip image with astrometric correction terms and uncertainties. 12,008,634 rows.

- **Exposure**. Information for each unique exposure with zero-point values and uncertainties. 255,454 rows.

- **Object**. Information on each unique object with average photometric, astrometric and morphology values. 2,930,644,736 rows.

- **Measurement**. Information on each individual source measurement. 34,658,213,888 rows. This table will be available as soon as is feasible.

- **Crossmatch**. Crossmatch information between the NSC and other large catalogs.

5. EXAMPLE SCIENCE USE CASES

5.1. *Dwarf Galaxies*

The Milky Way is orbited by faint dwarf galaxy satellites that can be challenging to detect. The best method to discovery these objects has been with resolved stellar populations as recently demonstrated by Bechtol et al. (2015) and Drlica-Wagner et al. (2015) using DECam data from the Dark Energy Survey. The NSC includes data of resolved stellar populations for regions of the sky previously unexplored for dwarf galaxies.

5.2. *Stellar Streams*

The Milky Way halo hosts a number of stellar streams from tidally stripped galaxies and globular clusters. One of the most famous streams is the Sagittarius stellar stream (e.g., Majewski et al. 2003; Koposov et al. 2012) that stretches more than 360° around the sky. Under the currently-favored hierarchical galaxy formation model, galaxies like our Milky Way are formed through the continual merging and accretion of smaller galaxies. The streams that we currently see are relics of this process. Studying these streams can help us understand how our galaxy was formed and its accretion history. The NSC covers regions of the sky that have not yet been explored for stellar streams.

5.3. *The Variable Sky*

Many astronomical objects vary with time either in their brightness or position in the sky. The temporal information in the NSC can be used to investigate the photometric and astrometric variability of objects. The NSC has 10,000 square degrees with ∼20 exposures, 200 square degrees with ∼100 exposures and 10 square degrees with at ∼1000 exposures (also see Figures 4 and 5). This kind of data content, combined with priors based on population statistics (Narayan et. al. 2018), will suffice to provide probabilistic classifications for a large fraction of known variable types.

- Variable stars, such as RR Lyrae, are essentially standard candles and are used to explore stellar structures in the Milky Way halo. The NSC sensitivity to RR Lyr stars extends throughout the Milky Way and its satellites.

- Active Galactic Nuclei (AGN) host supermassive black holes at the centers of galaxies and investigating their photometric variability can be used to study the accretion history of material onto the
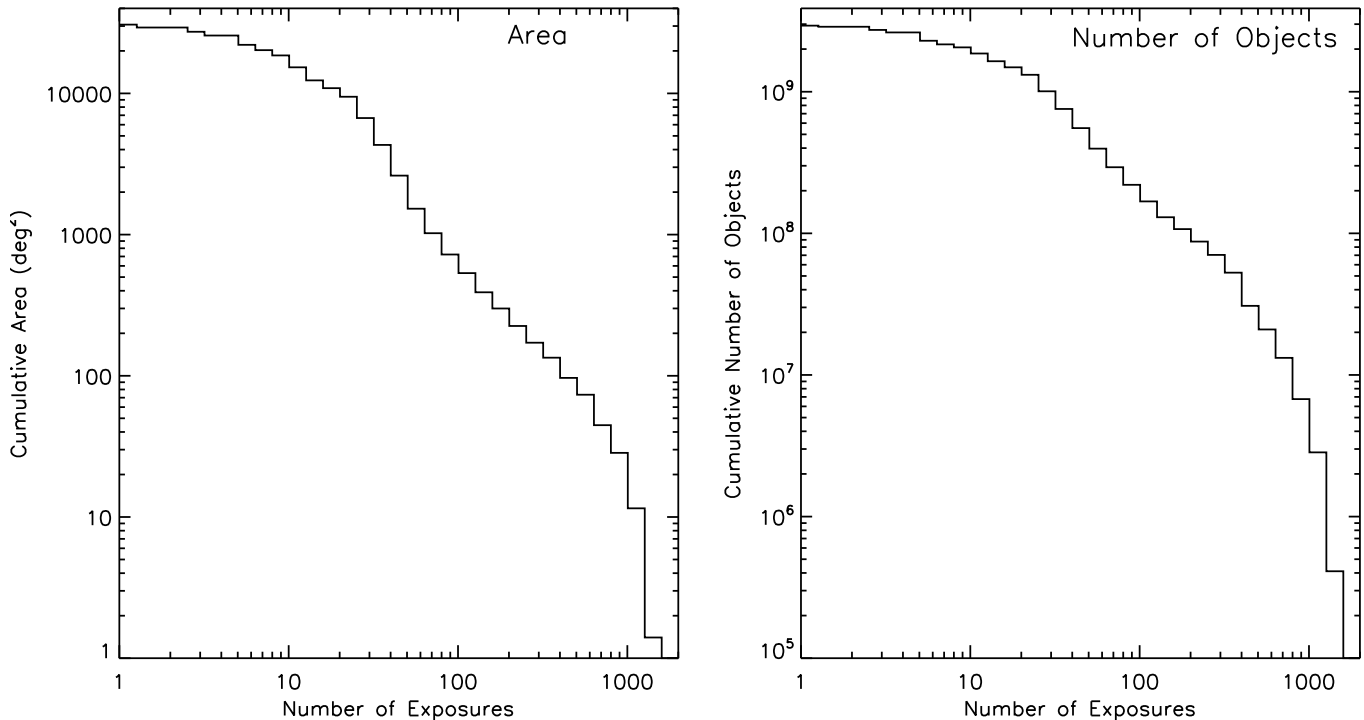
Fig. 5.— Cumulative histogram of (*Left*) area and (*Right*) number of objects with numbers of exposures greater than some value.

black hole, estimate the black hole mass, and explore the structure of the broad emission-line region.

- Transient events, like supernova explosions can be used to study interesting astrophysical phenomena as well as the expansion of the universe. NSC images document the "before" star fields of future SNe.

- Proper motions of objects can be used to identify moving groups of stars in the Milky Way galaxy and to select nearby, low luminosity objects by there large apparent motion.

The NSC information can be used to study all of these phenomena across nearly the entire sky.

NSC provides 1000 images for $\sim 2 \times 10^6$ targets, and 100 images for $\sim 2 \times 10^8$ targets. This is sufficient to investigate brighter examples of the most numerous object types for which LSST will provide variability details, and to evaluate predictions of target counts.

A simple binary population model (Ridgway et al. 2014a) shows that faint, potentially interacting high-energy binary systems should be numerous, up to ~ 1000 per deg^2 at mid-galactic latitudes. It is not known what fraction of these may provide detectable outbursts with what frequency, and the NSC can constrain this fraction.

Predictions for the content of the variable sky (Ridgway et al. 2014b) indicate that at the NSC depth, the sky should contain ~ 100 detectably variable QSOs, and ~ 500 detectably variable AGN per deg^2 – predictions that can be refined with NSC statistics.

5.4. *Synoptic Sky Surveys*

The NSC performance of $\sim$23rd magnitude at $\sim 5\sigma$ will be a good match for the synoptic survey capability of the Zwicky Transient Factory (Bellm et al. 2015), which is projected to have a limiting magnitude $\sim$20.5. Most detectably variable objects are galactic stars, and the NSC can catalog a large fraction of those. NSC photometry will provide valuable color and variability diagnostics for common galactic transient types such as flares from cool dwarfs and outbursts of cataclysmic variables. In addition, the NSC can be used to provide characteristics of host galaxies for extragalactic variability phenomena such as AGN, QSOs and Tidal Disruption Events. NSC can provide historical evidence that candidate SNe are in fact blank field transients, and not outbursts of known objects. NSC can also provide supplemental variability information, with a longer temporal baseline, for all observed source types. Finally, the NSC will also serve as a good first epoch of astrometric data for surveys like LSST which will allow for the measurement of accurate proper motions for objects fainter than Gaia's magnitude limit.

5.5. *Solar System Objects*

The NSC temporal information can be used to detect solar system objects. Undoubtedly, trans-Neptunian objects detected in the NSC catalog remain to be identified. There is a large interest in finding near earth objects that could potentially impact the earth, and NSC can be used to "precover" objects that will be discovered in future surveys. In addition, there is a big search for Planet 9 (Batygin & Brown 2016)[11] and if it exists the proof could be lurking inside the NSC.
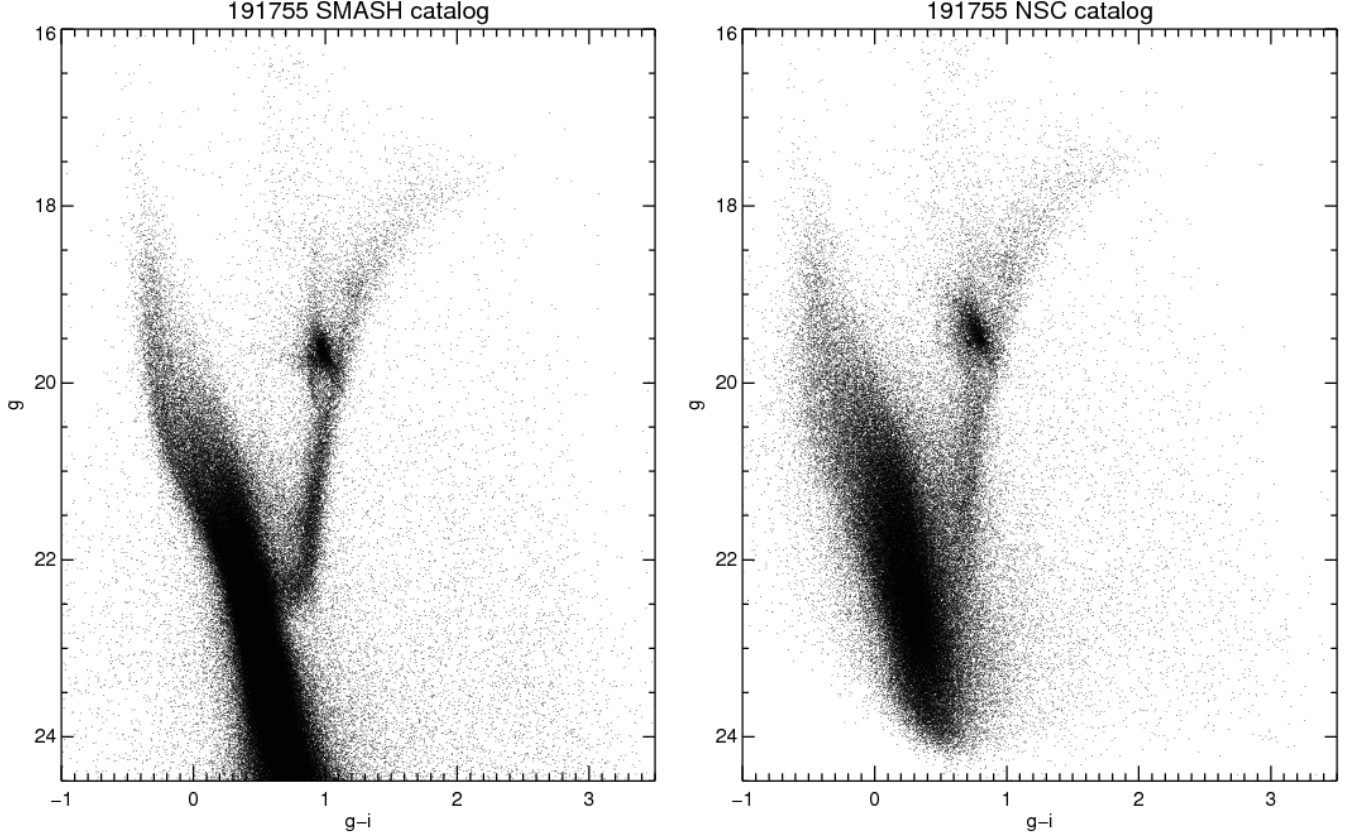
---

[11] http://www.findplanetnine.com

FIG. 6.— CMD comparison for healpix pixel 191755 at a radius of 2.4° from the LMC center. *(Left)* SMASH photometry. *(Right)* NSC photometry.
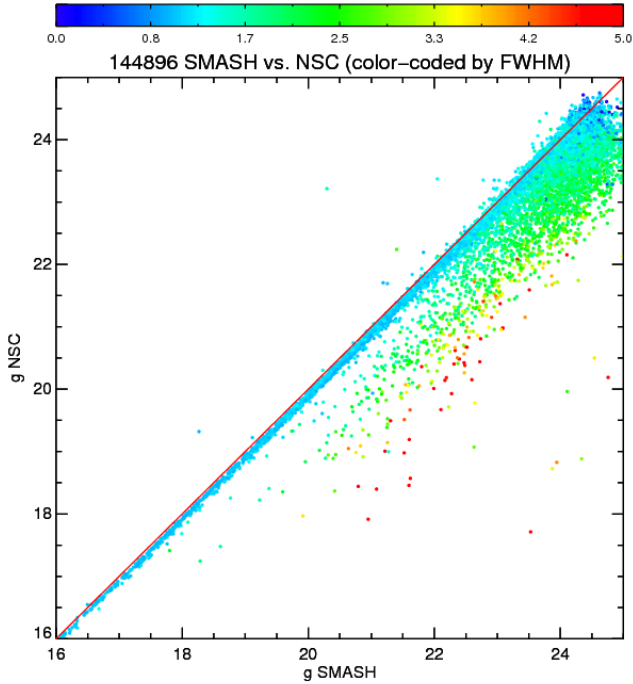

FIG. 7.— Direct *g*-band one-to-one comparison of SMASH and NSC photometry in the healpix pixel 144896 color-coded by an object's FWHM. The one-to-one line is shown in red.

6. FUTURE PLANS

For the first data release of the NSC we took the approach to start very simple and once we understood the main steps we would increase the complexity of the analysis. Here are some of the improvements we plan to make in the future:

- Improved photometric calibration in the south: SkyMapper data will be used for photometric calibration once it becomes available and should improve the photometric accuracy. This should also allow for chip-level zero points.

- Improved proper motions: The current proper motions are relative to the foreground stars and limited to $\lesssim 200$ mas yr^{-1} because of the 0.5″ matching radius used in the combination step. In the future, the proper motions will be put on an absolute scale by either applying position-dependent correction terms or by using an astrometric reference frame (e.g., QSOs) and an improved matching radius will be used.

- Improved photometric variability index: Better photometric variability quantities will be computed including the χ^2 and probability value of the object being photometrically constant and possibly Lamb-Scargle like metrics.

- PSF photometry of individual exposures: PSF photometry will be performed on the individual images possibly with SExtractor and PSFEx.
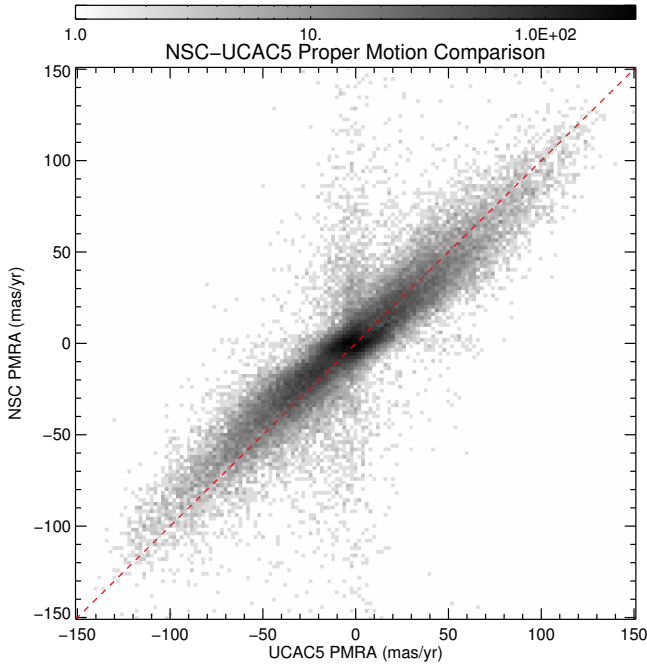
Fig. 8.— Comparison of NSC proper motions to those from UCAC5. The S/N of the proper motion measurement was required to be higher than 3 or the proper motion error less than 3 mas yr^{-1} in both catalogs. The one-to-one line is shown in red.

6.1. *Summary*

We present the first public data release of the NOAO Source Catalog (NSC) that contains the majority of the public imaging data in the NOAO Science Archive from both the northern and southern hemispheres. The NSC covers ∼30,000 square degrees, contains over 2.9 billion unique objects with 34 billion individual measurements to a depth of ∼23rd magnitude. With a baseline of ∼5 years and tens to thousands of exposures per object and an accuracy of the astrometric zero point of ∼2 mas the NSC provides precise proper motions for many objects. The NSC will be useful for exploring Galactic structure by searching for dwarf satellite galaxies, stellar streams and mapping variable stars. In addition, the temporal component of the NSC will allow for interesting time-series studies including searches for transients, investigations of AGN variability, and searches for solar system objects. The NSC will also serve as a good astrometric and photometric first epoch for future synoptic surveys like ZTF and LSST. Future improvements to the NSC include PSF photometry of individual and stacked images as well as real-time updates to the catalog as new images become public.

- PSF photometry of coadd images: Coadd images will be created for each band and PSF photometry performed on them.

- Forced photometry: Once the coadd photometry catalogs exist, it will be possible to perform forced photometry on the individual images.

- Real-time updates: Instead of regular data releases on an annual or bi-annual timescale, the catalog will be updated in real-time as new exposures become public.

- Catalog-level transient detection: Transients can be detected at the catalog level if the photometry can be produced fast enough (<1 day).

REFERENCES

https://www.theatlantic.com/technology/archive/2012/04/how-big-data-is-changing-astronomy-again/255917/
Batygin, K., & Brown, M. E. 2016, AJ, 151, 22
Bechtol, K., Drlica-Wagner, A., Balbinot, E., et al. 2015, ApJ, 807, 50
Bellm, E. C., Kulkarni, S. R., & ZTF Collaboration 2015, American Astronomical Society Meeting Abstracts, 225, 328.04

Bertin, E., & Arnouts, S. 1996, A&AS, 117, 393
Bianchi, L., Herald, J., Efremova, B., et al. 2011, Ap&SS, 335, 161
Bijaoui, A., & Dantel, M. 1970, A&A, 6, 51
Brunner, R. J., Djorgovski, S. G., Prince, T. A., & Szalay, A. S. 2002 Massive Computing, 4, 931
Dark Energy Survey Collaboration, Abbott, T., Abdalla, F. B., et al. 2016, MNRAS, 460, 1270

Dey, A., Rabinowitz, D., Karcher, A., et al. 2016, Proc. SPIE, 9908, 99082C

Drlica-Wagner, A., Bechtol, K., Rykoff, E. S., et al. 2015, ApJ, 813, 109

Gaia Collaboration, Brown, A. G. A., Vallenari, A., et al. 2016, A&A, 595, A2

Henden, A. A., Levine, S., Terrell, D., & Welch, D. L. 2015, American Astronomical Society Meeting Abstracts, 225, 336.16

Ivezic, Z., Tyson, J. A., Abel, B., et al. 2008, arXiv:0805.2366

Jannuzi, B. T., & Dey, A. 1999, Photometric Redshifts and the Detection of High Redshift Galaxies, 191, 111

Koposov, S. E., Belokurov, V., Evans, N. W., et al. 2012, ApJ, 750, 80

Magnier, E. A., Schlafly, E. F., Finkbeiner, D. P., et al. 2016, arXiv:1612.05242

Majewski, S. R., Skrutskie, M. F., Weinberg, M. D., & Ostheimer, J. C. 2003, ApJ, 599, 1082

Martin, N. F., Nidever, D. L., Besla, G., et al. 2015, ApJ, 804, L5

McConnachie, A. W. 2012, AJ, 144, 4

Narayan, G., Zaidi, T., Soraisam, M. D., Wang, Z., et al. 2018, ApJ, in press

Nidever, D. L., Olsen, K., Walker, A. R., et al. 2017, AJ, 154, 199

Ridgway, S. T., Matheson, T., Mighell, K. J., & Howell, S. B. 2014, ApJ, 796, 53

Ridgway, S. T., Matheson, T., Mighell, K. J., & Howell, S. B. 2014, ArXiv e-prints, arXiv:1409.3265

Schlegel, D. J., Finkbeiner, D. P., & Davis, M. 1998, ApJ, 500, 525

Skrutskie, M. F., Cutri, R. M., Stiening, R., et al. 2006, AJ, 131, 1163

Valdes, F., Gruendl, R., & DES Project 2014, Astronomical Data Analysis Software and Systems XXIII, 485, 379

York, D. G., Adelman, J., Anderson, J. E., Jr., et al. 2000, AJ, 120, 1579

Zacharias, N., Finch, C., & Frouard, J. 2017, AJ, 153, 166

Zhang, Y. & Zhao, Y. 2015 Data Sci J 14,11

Zou, H., Zhou, X., Fan, X., et al. 2017, PASP, 129, 064101